Jorge D'Elía
Graduate Researcher,
e-mail: jdelia@intec.unl.edu.ar

Mario A. Storti
Senior Researcher,
e-mail: mstorti@intec.unl.edu.ar

Sergio R. Idelsohn
Professor,
e-mail: rngtm@acride.edu.ar

Centro Internacional de Métodos Computacionales en Ingeniería (CIMEC), INTEC (UNL-CONICET). Güemes 3450, 3000-Santa Fe, Argentina

A Panel-Fourier Method for Free-Surface Flows

A panel-Fourier method for ship-wave flow problems is considered here. It is based on a three-dimensional potential flow model with a linearized free surface condition, and it is implemented by means of a low order panel method coupled to a Fourier-series. The wave-resistance is computed by pressure integration over the static wet hull and the wave-pattern is obtained by a post-processing procedure. The strategy avoids the use of numerical viscosity, in contrast with the Dawson-like methods, widely used in naval-panel codes, therefore a second centered scheme can be used for the discrete operator on the free surface. Numerical results including the wave-pattern for a ferry along fifteen ship-lengths are presented. [S0098-2202(00)01402-4]

1 Introduction

Panel methods are classical and widely accepted in the industry for calculating potential flows, e.g., Morino and Kuo, [1], Katz and Plotkin [2]. In some problems a two-dimensional approach is sufficient, for instance, flows past multicomponent airfoils, infinite cascade and ground effects, e.g., Mokry [3], Storti et al. [4] while in others a three-dimensional approach is necessary. Earlier panel methods were of nonlifting type, which have served as a basis for their lifting successors. Since most subsequent panel developments carried out by aircraft-oriented investigators for whom the lift and the wake are all-important, principal attention was focused on the means of handling them (e.g., Morino [5]). Marine problems, like the flow around propellers, can be also treated by the same methods (e.g., Kinnas and Hsin [6]). However, many of them are truly nonlifting, such as the case of surface ships (e.g., Dawson [7]) and, then, in these problems, where the nonlifting case has received a most extensive development and industrial use. More recently, ship-wake and wave-pattern far downstream are also of interest due to satellite remote sensing. In general, the hydrodynamic problem retains many of the complexities associated with aircraft case such as the need to predict the flow around multiple bodies, for instance, the fuselage/wing interaction can be seen as equivalent to hull/keel interaction. Other approaches are also possible as multigrid Euler schemes with artificial compressibility (e.g., Farmer et al. [8]). In the surface ship case, when a body moves near the free surface of a fluid, a pattern of trailing gravity waves is formed. The energy spent in building this pattern comes from the work done by the body against the *wave resistance*. As a first approximation, the wave resistance can be computed using a potential model, while for the viscous drag it can be assumed that the position of the surface is held fixed at the reference hydrostatic position, i.e., a plane. This is, basically, the *Froude hypotheses*. With this assumption the interaction produced between the boundary layer (which tends to produce a larger body) and the wave pattern is neglected. Even if a potential model is assumed for the liquid, the problem is nonlinear due to the free surface boundary condition.

This work focuses in the computation of the flow field and wave resistance for a body in steady motion on deep water by means of a potential model for the fluid and a linearized free surface boundary condition. This is the basis for most ship design codes in industry. The governing equations are the Laplace equation with slip boundary conditions on the hull and channel walls, inlet/outlet conditions at the corresponding planes and the free surface boundary conditions. At this stage, the mathematical model results in a nonlinear one due to both kinematic and dynamic boundary conditions on the free surface (e.g., see Stoker, [9]). The first of them is related to the unknown position of the free surface, while the second one is related to the nonlinear expression of the Bernoulli equation. A classical strategy in hydrodynamic theory is to make use of asymptotic expansion (e.g., see van Dyke, [10]). In this case, the flow equations are parameterized with respect to an expansion parameter, for example, the Froude number or some of the draft/length and beam/length relations. Then, a *basic* flow is solved which is obtained by taking some limit process on the parameterized equations, so a simpler flow problem is obtained. Finally, a *perturbed* flow is solved, where the perturbation is assumed small enough to remain valid the asymptotic procedure, and usually it is sufficient to stop this procedure at this point. A number of linearizations assuming expansion in the aforementioned parameters can be found in ship hydrodynamic, see e.g., Newman [11]. But the most useful are those related to the slow ship (small Froude number), where the (composed) free surface boundary condition of the perturbed flow amounts to a Neumann boundary condition with a source term proportional to the streamlined second derivative of the basic potential flow. However, without radiation boundary conditions the hydrodynamic problem as stated so far is not well posed, since it is invariant under longitudinal coordinate inversion ($x \rightarrow -x$), and, therefore, unable to capture the characteristic trailing waves propagating downstream. To correct this deficiency, it can be either add a dissipative numerical mechanism or impose some kind of *absorbing* boundary condition. The addition of a third-order derivative to the free surface boundary conditions results equivalent to add a dissipative mechanism and captures the correct sense of propagation for the wave pattern. This is equivalent to the use of a noncentered discretization scheme for the second order operator and falls among the well known *upwind* techniques, e.g., see Baumann et al. [12] or Nigro et al. [13]. The amount of added viscosity is related to the length of the mesh downstream of the body. If the viscosity parameter is too low, the trailing waves arriving at the downstream boundary, are reflected in the upstream direction and pollute the solution. On the other hand, if it is too high, the trailing waves are damped, and incorrect values of the wave-resistance are obtained. Extending the mesh in the down-

Contributed by the Fluids Engineering Division for publication in the JOURNAL OF FLUIDS ENGINEERING. Manuscript received by the Fluids Engineering Division May 27, 1998; revised manuscript received November 30, 1999. Associate Technical Editor: P. Bandyopadhyay.

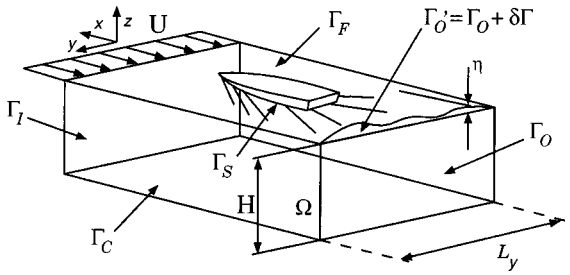

Fig. 1 Geometrical description of the ship wave-resistance problem

stream direction allows the use of a lower viscosity parameter, since the waves are damped over a longer distance, but increases the computational cost (core memory). Numerical experience shows that this third-order streamline viscosity term is too dissipative and the meshes should be extended downstream too much. Dawson proposed a method, where a fourth order derivative (in a velocity formulation) is used instead, with a very particular finite difference discretization. It is astonishing that standard discretization of the same operator does not work and neither do higher order operators (say to the seventh order). As a result, most of today's industrial hydrodynamic codes are still using some kind of variant of the Dawson scheme. However, this very particular viscosity term is hard to extend to general boundary fitted meshes, let alone unstructured computational methods like finite elements. Due to this cause most codes are based on a highly structured panel formulation. Another possibility is to use an *absorbing* boundary condition in the downstream boundary. If such a numerical device were found, then there would be no need to add a numerical viscosity term since the trailing waves are not reflected upstream, and a standard second order centered scheme can be used for the free-surface boundary term. Absorbing boundary conditions have been throughly studied for other wave phenomena like the Helmholtz equation, as the DtN (Givoli and Keller [14]) or the DNL (Bonet et al. [15]). For the ship-wave resistance problem the absorbing boundary conditions are seldom used due to inherent difficulties in its development. Recently, Storti et al. [16–18] have proposed a method with a finite element approach, while Broeze and Romate [19] developed an absorbing boundary condition with a panel method in the context of a temporal evolution of the free surface.

The general objective of this work is the development of a numerical method for the ship-wave flow potential problem with centered schemes in contrast to the Dawson-like methods. This is done by a panel method coupled with a finite Fourier series and discrete nonlocal absorbing boundary conditions. On the one hand, periodic boundary conditions on the beam direction are assumed and, then, the asymptotic wave-potential is represented by a superposition of monochromatic-waves. On the other hand, it is assumed that the mesh is structured both at the upstream and downstream sides with a finite number of strips in the beam direction. Then, additional boundary equations are introduced which are based on the flow kinematics at the upstream and downstream boundaries taking into account the right sense of the wave pattern, so that a second *centered* scheme can still be used for the discrete free surface operator.

2 Formulation of Potential Flow

The flow around a ship moving at a constant speed in a channel of uniform section is considered. It is supposed, for simplicity, that the channel section is a rectangle of depth H and width L_y, as shown in Fig. 1. The fluid occupies the region Ω which is bounded by: the channel walls and bottom Γ_C, the inlet/outlet boundaries $\Gamma_{I/O}$, the wetted surface of the ship Γ_S and the free surface Γ_F. The x-axis is parallel to the upstream nonperturbed velocity $\mathbf{u}_\infty$ and the z-axis positive upwards. The velocity field $\mathbf{u}$ is given by $\mathbf{u}=\nabla\Phi$, where Φ is the total potential, which satisfies the Laplace equation in the flow domain Ω. It is split as $\Phi=\mathbf{u}_\infty^T\mathbf{x}+\phi$ where $\mathbf{x}=(x,y,z)$ is the position vector and ϕ is the perturbation potential. The position of the free surface Γ_F is given by the single valued function $z=\zeta(x,y)$, where ζ is the elevation of the free surface with respect to the reference plane $z=0$ which is the hydrostatic equilibrium plane.

2.1 Kinematic Boundary Condition. The kinematic boundary condition is the slip condition $\partial_n\Phi=0$ at the wetted body surface, channel walls, bottom and free surface. Alternatively, Dirichlet boundary conditions at the bottom can be considered, e.g., see Storti et al. [16]. The unit normal to the free surface $z=\zeta(x,y)$ is expressed as $\mathbf{n}=(n_x,n_y,n_z)=(-\zeta_{,x},-\zeta_{,y},\mathbf{1})$.

2.2 Dynamic Boundary Condition. An additional condition must be added to the Laplace equation and the kinematic boundary conditions, since the position ζ of the free surface is not known beforehand. This is done by means of the Bernoulli equation

$$\frac{p}{\rho}+\frac{1}{2}|\nabla\phi|^2+g\zeta=C \quad \text{in } \Omega; \tag{1}$$

which relates the pressure p, the velocity $\nabla\Phi$ and the height ζ. The vapor pressure and the surface tension of the water are disregarded, therefore the mechanical equilibrium on the air/water interface requires that the pressure p be equal on both sides of them, and equal to the atmospheric pressure p_{atm} which is also assumed to be constant. Then, at infinity upstream, $C=p_{\text{atm}}/\rho+u_\infty^2/2$ and, without loss of generality, $p_{\text{atm}}=0$ is adopted.

2.3 Radiation Boundary Conditions. Roughly speaking, the radiation boundary conditions should allow the energy to flow, in the form of radiating waves propagate downstream and exit cleanly at Γ_O. In contrast, no waves are allowed to propagate upstream to Γ_I so that the boundary condition imposes that the potential should approach the undisturbed one on this boundary. Note that, the different treatment in Γ_I and Γ_O is the unique element that determines the symmetry breaking $x\to -x$, and ensures a physically correct wave pattern.

2.4 Governing Equations. The governing equations for the solution $\{\Phi,\zeta\}$ of this model are:

$$\begin{cases} \Delta\Phi=0 & \text{in } \Omega; \\ \partial_n\Phi=0 & \text{at } \Gamma_S+\Gamma_C; \\ \zeta=(u_\infty^2-|\nabla\Phi|^2)/(2g) & \text{at } \Gamma_F; \\ -\zeta_{,x}\Phi_{,x}-\zeta_{,y}\Phi_{,y}+\Phi_{,z}=0 & \text{at } \Gamma_F; \\ |\nabla\Phi|<\infty & \text{at } \Gamma_{I,O}. \end{cases} \tag{2}$$

3 Slow Ship Expansion

Asymptotic expansions for this flow problem, usually, consider some of the following parameters: the draft relation $\lambda_H=H/L$, the beam relation $\lambda_B=B/L$ or the Froude number $\text{Fr}=U/\sqrt{gL}$, which conduce to the known linearizations of: the *slender* ship when $\lambda_{H,B}\ll 1$, the *thin* ship when $\lambda_B\ll 1$, the *slow* ship when $\text{Fr}\ll 1$ and, of course, some combinations of them. The only case considered here is the slow ship on deep water, where its basic flow is obtained by taking the limit $g\to\infty$ and, then, the free surface $\zeta(x,y)$ shrinks to the hydrostatic equilibrium plane $z=0$, as it immediately follows from inspection of the dynamic boundary condition. That is, the wave-pattern behind the ship is missing, and is also equivalent to a *double body* flow obtained by mirroring the flow regime with respect to the plane $z=0$. After solving the basic flow, the gravity acceleration is restarted to its original value. If the wave heights are small enough, then they would be seen as a perturbation of the basic flow (e.g., see Reference [11]), whose

mathematical treatment, at a first stage, leads to a linearization of the governing equations following some kind of approach on the free surface. Next, a linearized expansion of the dynamic and kinematic boundary conditions over the free surface for the slow ship is considered. The *k*-solution of a perturbation procedure is $\{\phi_k,\zeta_k\}$, potential and elevation, respectively. Here $k=0$ corresponds to the *basic* flow problem and $k=1$ is the *perturbed* flow. In order to obtain the pair solution $\{\phi_1,\zeta_1\}$ an asymptotic expansion is made, $\{\phi_1,\zeta_1\}=\{\phi_0+\psi\varepsilon,\zeta_0+\eta\varepsilon\}$, at first order in ε, with $\varepsilon=\mathrm{Fr}$ and $0<\varepsilon\ll 1$ for the slow ship, where $\{\psi,\eta\}$ is the (incremental) wave-pair solution composed by the wave-potential ψ and the wave-height η. Both potentials $\phi_{0,1}$ are harmonic, $\Delta\phi_{0,1}=0$, in their respective domains $\Omega^{0,1}$, and it will be also assumed that the elevations $\zeta_{0,1}$ are single valued and small enough, so the resulting pair of incremental solutions $\{\varepsilon\psi,\varepsilon\eta\}=\{\phi_1-\phi_0,\zeta_1-\zeta_0\}$ are also small enough when $\varepsilon\ll 1$. The linearized dynamic and kinematic boundary conditions can be expressed in terms of the wave-pair solution $\{\psi,\eta\}$ and they are derived in the Appendix.

4 Linearized Wave-Potential

The linearized perturbed system for the incremental wave-pair solution $\{\psi,\eta\}$ can be written as:

$$\begin{cases} \Delta\psi=0 & \text{in } \Omega; \quad (3a)\\ \partial_n\psi=0 & \text{at } \Gamma_S+\Gamma_C; \quad (3b)\\ g\eta=-\mathbf{U}_0^T\nabla\psi-r_0 & \text{at } z=0; \quad (3c)\\ \partial_n\psi=\nabla^T(\mathbf{U}_0\eta) & \text{at } z=0; \quad (3d)\\ |\nabla\psi|<\infty & \text{at } \Gamma_{I,0}. \quad (3e) \end{cases}$$

where $\mathbf{U}_0=\mathbf{u}_\infty+\nabla\phi_0$ is the velocity field over the hydrostatic plane $z=0$ and r_0 is the residue of the dynamic boundary condition of the basic flow. Replacing (3*c*) in (3*d*)

$$\partial_n\psi=-\frac{1}{g}\nabla^T\mathbf{U}_0\mathbf{U}_0^T\nabla\psi-\frac{1}{g}\nabla^T\mathbf{U}_0 r_0. \quad (4)$$

The residue r_0 is found writing the Bernoulli equation (with $\rho=1$) for the basic flow

$$\frac{1}{2}U_0^2+g\zeta^0=\frac{1}{2}u_\infty^2+r_0; \quad (5)$$

where $\mathbf{\Phi}_0=\mathbf{u}_\infty^T\mathbf{x}+\phi_0$ is the total potential of the basic flow, but, in this case, the free surface coincides with the hydrostatic plane $\zeta^0=z=0$, and from this $r_0=(U_0^2-u_\infty^2)/2$, where $U_0^2=|\nabla\mathbf{\Phi}_0|^2$. Then

$$\partial_n\psi=-\frac{1}{g}\nabla^T\mathbf{U}_0\mathbf{U}_0^T\nabla\psi-\frac{1}{2g}\nabla^T\mathbf{U}_0(U_0^2-u_\infty^2) \quad (6)$$

is a nonhomogeneous Neumann boundary condition (at $z=0$) for the wave-perturbation potential ψ, and it can be seen as a *transpiration* flow $\sigma'\equiv\partial_n\psi$ that is injected to simulate the displacement of the free surface from the hydrostatic plane $z=0$. Therefore

$$\begin{cases} \sigma'=D\psi+f;\\ D=-1/g\nabla^T\mathbf{U}_0\mathbf{U}_0^T\nabla;\\ f=-1/(2g)\nabla^T\mathbf{U}_0(U_0^2-u_\infty^2). \end{cases} \quad (7)$$

5 Panel Formulation

The panel solution is carried out in two steps. First, the basic flow problem is solved and, then, the perturbed one. For both steps the same panel mesh is employed, where the free surface portion coincides with the hydrostatic equilibrium portion over the plane $z=0$. The zero-order panel mesh is a polyhedric one with flat faces, $\Gamma_n=\Gamma_p\cup\Gamma_b$, being Γ_p the mesh with n_p panels over a finite portion of the free surface Γ_F and Γ_b the mesh with n_b panels over the wetted body surface. The total number of panels is $n=n_p+n_b$ where, usually, $n_p\gg n_b$. The panel numeration should be correlative for an easy block-matrix treatment, starting with the free surface Γ_p. A low order panel formulation for both flow cases is employed, with collocation at the centroids of the panels, to set up a linear system of algebraic equations, where the system matrix is square of dimension $N=n$ for the basic flow, and $N=n+2n_y$ for the perturbed one, with $n_y\ll n$.

5.1 Panel Method for the Basic Flow. The system of equations for the basic flow problem is written as $\mathbf{A}\boldsymbol{\mu}^0=\mathbf{b}^0$, where $\mathbf{A}$ is the (bipolar) matrix system, and $\boldsymbol{\mu}^0$ and $\mathbf{b}^0$ are the basic potential and source vectors, respectively, evaluated at the centroids of the *n*-panels. The source vector $\mathbf{b}^0=\mathbf{C}\boldsymbol{\sigma}^0$ is the product of the monopolar influence matrix $\mathbf{C}$ and the flow vector $\boldsymbol{\sigma}^0$ obtained by means of the *slip* boundary condition on the solid walls, $\sigma^0(\mathbf{x}_j)=-\mathbf{U}_0^T(\mathbf{x}_j)\mathbf{n}(\mathbf{x}_j)$, where $\mathbf{n}(\mathbf{x}_j)$ is the *j*-unit panel normal oriented to the wetted side. The bipolar and monopolar matrices $\mathbf{A}$ and $\mathbf{C}$ are given by the surface integrals

$$A_{ij}=\frac{1}{4\pi}\int_\Gamma d\Gamma_j\frac{\mathbf{r}_{ij}^T\mathbf{n}_j}{r_{ij}^3} \text{ and } C_{ij}=\frac{1}{4\pi}\int_\Gamma d\Gamma_j\frac{1}{|\mathbf{r}_{ij}|}, \quad (8)$$

where $\mathbf{r}_{ij}=|\mathbf{x}_i-\mathbf{x}_j|$ is the distance between the centroid $\mathbf{x}_i$ and the integration point $\mathbf{x}_j$ over the *j*-panel surface, and $\mathbf{x}=(x,y,z)$. These discrete integrals are evaluated in closed form following a rotational strategy, e.g., see Medina and Liggett [20], D'Elía [21], or D'Elia et al. [22–24]. The matrix system is split in a plane-body block fashion

$$\begin{bmatrix}\mathbf{A}_{pp} & \mathbf{A}_{pb}\\ \mathbf{A}_{bp} & \mathbf{A}_{bb}\end{bmatrix}\begin{bmatrix}\boldsymbol{\mu}_p^0\\ \boldsymbol{\mu}_b^0\end{bmatrix}=\begin{bmatrix}\mathbf{C}_{pp} & \mathbf{C}_{pb}\\ \mathbf{C}_{bp} & \mathbf{C}_{bb}\end{bmatrix}\begin{bmatrix}\boldsymbol{\sigma}_p^0\\ \boldsymbol{\sigma}_b^0\end{bmatrix}. \quad (9)$$

5.2 Panel Method for the Perturbed Flow. For the perturbed flow problem all the surfaces remain fixed and the same panel mesh is employed. A lineal system similar to the previous one is written. The Neumann boundary condition is split in two components: a null part over the body $\boldsymbol{\sigma}_b=\mathbf{0}$ and

$$\boldsymbol{\sigma}_p=\mathbf{D}_{pp}\boldsymbol{\mu}_p+\mathbf{f}; \quad (10)$$

over the free surface, where $\mathbf{D}_{pp}=\mathrm{diag}(D_i)$, with $D_i=D(\mathbf{x}_i)$, is the free-surface matrix and $f_i=f(\mathbf{x}_i)$ is the forcing vector. Replacing $\boldsymbol{\sigma}_p$ and $\boldsymbol{\sigma}_b$ and rearranging

$$\begin{bmatrix}(\mathbf{A}_{pp}-\mathbf{C}_{pp}\mathbf{D}_{pp}) & \mathbf{A}_{pb}\\ (\mathbf{A}_{bp}-\mathbf{C}_{bp}\mathbf{D}_{pp}) & \mathbf{A}_{bb}\end{bmatrix}\begin{bmatrix}\boldsymbol{\mu}_p\\ \boldsymbol{\mu}_b\end{bmatrix}=\begin{bmatrix}\mathbf{C}_{pp}\mathbf{f}\\ \mathbf{C}_{bp}\mathbf{f}\end{bmatrix}; \quad (11)$$

and it remains to introduce the radiation boundary conditions upstream and downstream since, otherwise, the hydrodynamic problem is not well posed.

5.3 Free Surface Matrix. A discrete version for the scalar operator $\nabla^T\mathbf{U}_0\mathbf{U}_0^T\nabla$ can be obtained with several approaches, for example finite/differences or mesh-less methods. But in any case it will have a compact stencil and the free surface matrix will be quite sparse. Then, the computational cost of evaluating the matrix right product $\mathbf{CD}$ with the (dense) monopolar influence matrix $\mathbf{C}$, will not be expensive if the operations are conveniently rearranged. The artificial viscosity schemes, such as upwind or Dawson-like methods, are usually introduced in the free surface matrix $\mathbf{D}_{pp}$, while for the proposed method a second order *centered* scheme can still be used for the discrete operator. For instance if $\mathbf{U}_0=(U,0,0)\approx\mathrm{cnst}$ over a structured mesh (x_i,y_j) on the free surface, with $n_x\times n_y$ nodes and mesh steps h_x,h_y, then, it can be estimated that $(\mathbf{D}_{pp}\boldsymbol{\mu})_{p,q}\approx-U^2/g\,\partial_{xx}\mu|_{p,q}$, where $p=i+1/2$, $q=j+1/2$, since the potentials are evaluated at the panel centroids, and

$$\partial_{xx}\mu|_{p,q}\approx h_x^{-2}(\mu_{p-1,q}-2\mu_{p,q}+\mu_{p+1,q}). \quad (12)$$

6 Panel-Fourier Method

6.1 Finite Fourier Series. First, a two-dimensional flow is considered, from left to right with non-perturbed velocity U, around a ship-like body of characteristic length L situated at the origin, totally or partially submerged in the flow. The governing equations for the wave-potential $\hat{\mu}(x,z)$ (see e.g., Stoker [9]) and

$$\begin{cases} \nabla^2\hat{\mu} & \text{on } -\infty<z\leqslant 0; \\ \hat{\mu}_{,z}+(U^2/g)\hat{\mu}_{,xx}=0 & \text{at } z=0; \\ \hat{\mu} \text{ and } \partial_z\hat{\mu} \text{ bounded} & \text{for all } y,z. \end{cases} \tag{13}$$

Its asymptotic solution downstream and far enough from the body, are written as a linear combination of sines and cosines in the propagating direction x affected with a decreasing exponential in the draft direction z

$$\hat{\mu}(x,z)=Ae^{Kz}\sin(Kx)+Be^{Kz}\cos(Kx) \tag{14}$$

for $x>x_w$ and $z\leqslant 0$, where x_w is an abscissa far enough from the body, i.e., $0<L<x_w<\infty$, A,B are two arbitrary amplitude constants which are determined from the boundary conditions, and $K=g/U^2$ is the wave number related to the wavelength $\lambda=2\pi K^{-1}=2\pi(U^2/g)$. For the three-dimensional case an equivalent asymptotic solution is developed. This is done by imposing periodic boundary conditions in the beam direction, and is equivalent to an infinite cascade of ship-like bodies with transversal disposition to the mean stream. Then, a finite Fourier series is introduced in the strip $-L_y/2\leqslant y\leqslant L_y/2$ on a structured panel mesh with n_y transversal strips, which allow the asymptotic wave-potential to be $\tilde{\mu}(x,y,z)$ and its x-derivative $\tilde{\sigma}(x,y,z)=\partial_x\tilde{\mu}$ as

$$\tilde{\mu}=\sum_{q=0}^{m-1} e_q[A_q\sin(k_{xq}x)+B_q\cos(k_{xq}x)]\cos(k_{yq}y) + \sum_{q=1}^{m} e_q[C_q\sin(k_{xq}x)+D_q\cos(k_{xq}x)]\sin(k_{yq}y); \tag{15}$$

$$\tilde{\sigma}=\sum_{q=0}^{m-1} f_q[A_q\cos(k_{xq}x)-B_q\sin(k_{xq}x)]\cos(k_{yq}y) + \sum_{q=1}^{m} f_q[C_q\cos(k_{xq}x)-D_q\sin(k_{xq}x)]\sin(k_{yq}y) \tag{16}$$

where $m=n_y/2\geqslant 1$ is assumed, $e_q=e^{k_{zq}z}$, $f_q=k_{xq}e^{k_{zq}z}$, and A_q,B_q,C_q,D_q are the amplitude constants of the Fourier modes, k_{xq},k_{yq} are the Cartesian plane wave-numbers on the hydrostatic equilibrium plane and k_{zq} is the draft attenuation of each mode. It can be shown that this finite Fourier series evaluated at the centroid ordinates y_i satisfies the orthogonal conditions. Now, a relation between k_{xq}, k_{yq} and k_{zq} is needed.

6.2 Dispersion Relation. With the geometrical assumptions made above, the asymptotic wave-perturbation potential $\tilde{\mu}(x,y,z)$ has been represented as the linear superposition of traveling plane-waves $\mu_q(x,y,z)$ on the planes $z=\text{cnst}$, with exponential attenuation in the draft direction $z\leqslant 0$, that is,

$$\tilde{\mu}=\sum_{q=0}^{n_y/2} E_q\tilde{\mu}_q \quad \text{with} \quad \tilde{\mu}_q=e^{ik_{xq}x+ik_{yq}y+k_{zq}z} \tag{17}$$

with E_q being complex constants. By superposition each traveling wave must satisfy the Laplace equation in the domain Ω and the linearized free boundary condition at $z=0$

$$\begin{cases} \partial_{xx}\tilde{\mu}_q+\partial_{yy}\tilde{\mu}_q+\partial_{zz}\tilde{\mu}_q=0 & \text{on } \Omega; \\ \partial_{xx}\tilde{\mu}_q+K\partial_z\hat{\mu}_q=0 & \text{at } z=0. \end{cases} \tag{18}$$

From Eq. (18), the following discrete relations are found

$$\begin{cases} k_{yq}=2\pi q/Ly \\ k_{xq}=\sqrt{K^2/2+1/2\sqrt{K^4+4K^2k_{yq}^2}} \\ k_{zq}=k_{xq}^2/K \end{cases} \tag{19}$$

for $q=0,2,\ldots,n_y/2$. They can be seen as a sort of *dispersion* relation (since the x-coordinate can be regarded as time-like) between the Cartesian wave-numbers k_{xq},k_{yq} and the draft atenuation k_{zq} for each n_y-Fourier mode.

6.3 Absorbing Boundary Conditions. A finite portion of the basic free surface (plane $z=0$) is discretized by a structured mesh in $n_p=n_x\times n_y$ panels, where n_x,n_y are the panel numbers in the length and beam direction, respectively, with a panel numeration $l=(i-1)n_y+j$, for $1\leqslant i\leqslant n_x$ and $1\leqslant j\leqslant n_y$. Next, a vertical wall is introduced at $x=x_w$ far enough downstream from the body, with $0<L<x_w<\infty$, also discretized with a structured panel mesh in $n_w=n_y\times n_z$ panels, where n_z is the number of panels in the draft direction. On the other hand, the mesh *on* the body surface has n_b panels and can be *nonstructured*. The total number of panels is $n=n_p+n_b+n_w$ and the matrix system for the perturbed flow problem is

$$\begin{bmatrix} \hat{\mathbf{A}}_{pp} & \mathbf{A}_{pb} & \mathbf{A}_{pw} \\ \hat{\mathbf{A}}_{bp} & \mathbf{A}_{bb} & \mathbf{A}_{bw} \\ \mathbf{A}_{wp} & \mathbf{A}_{wb} & \mathbf{A}_{ww} \end{bmatrix} \begin{bmatrix} \boldsymbol{\mu}_p \\ \boldsymbol{\mu}_b \\ \boldsymbol{\mu}_w \end{bmatrix} = \begin{bmatrix} \mathbf{C}_{pp} & \mathbf{C}_{pw} \\ \mathbf{C}_{bp} & \mathbf{C}_{bw} \\ \mathbf{C}_{wp} & \mathbf{C}_{ww} \end{bmatrix} \begin{bmatrix} \mathbf{f} \\ \boldsymbol{\sigma}_w \end{bmatrix} \tag{20}$$

where

$$\begin{cases} \hat{\mathbf{A}}_{pp}=\mathbf{A}_{pp}-\mathbf{C}_{pp}\mathbf{D}_{pp}; \\ \hat{\mathbf{A}}_{bp}=\mathbf{A}_{bp}-\mathbf{C}_{bp}\mathbf{D}_{pp}; \end{cases} \tag{21}$$

and Eq. (10) was introduced. Neither $\boldsymbol{\mu}_w$ nor $\boldsymbol{\sigma}_w$ are known and, then, the system is under-specified. Next, a relation between them will be found through the absorbing boundary conditions. First, the n_y-Fourier modes on the vertical wall are introduced

$$\boldsymbol{\sigma}_j=\tilde{\boldsymbol{\sigma}}_j \quad \text{and} \quad \boldsymbol{\mu}_j=\tilde{\boldsymbol{\mu}}_j \tag{22}$$

for $j-n_p-n_b=1,2,\ldots,n_w$. As they already satisfy the governing equations, the last row of Eq. (20) is relaxed. The remaining set of equations in full length form are

$$\sum_{j=1}^{j_1}\hat{a}_{ij}\mu_j+\sum_{j=j_1+1}^{j_2}a_{ij}\mu_j+\sum_{j=j_2+1}^{n}a_{ij}\mu_j=b_j; \tag{23}$$

for $i=1,2,\ldots,(n_p+n_b)$, where $j_1=n_p$, $j_2=n_p+n_p$ and

$$b_j=\sum_{j=1}^{j_2}c_{ij}f_j+\sum_{j=j_2+1}^{n}c_{ij}\sigma_j. \tag{24}$$

Replacing from Eqs. (15), (16), and (20)

$$\sum_{j=1}^{j_1}\hat{a}_{ij}\mu_j+\sum_{j=j_1+1}^{j_2}a_{ij}\mu_j+\sum_{j=j_2+1}^{n}T_j=\sum_{j=1}^{j_1}c_{ij}f_j; \tag{25}$$

with

$$T_j=\sum_{q=1}^{n_y/2}(\alpha_{ijq}A_q+\beta_{ijq}B_q+\gamma_{ijq}C_q+\delta_{ijq}D_q). \tag{26}$$

There are $(n_p+n_b+2n_y)$ unknowns, but there are only (n_p+n_b) collocation equations, then $2n_y$ additional equations must be added for the Fourier amplitudes. Second, $2n_y$ kinematic boundary conditions are introduced upstream and downstream. At upstream, a *null* x-slope on each panel strip is imposed

$$-\mu_i+\mu_{n_y+i}=0 \quad \text{for } i=1,2,\ldots,n_y \tag{27}$$

while at downstream, compatability is imposed between the wave-potential and its asymptotic expansion on each panel strip, at the intersection between the free surface and the vertical wall

$$-\frac{1}{2}\mu_{i-n_y}+\frac{3}{2}\mu_i-\sum_{j=j_2+1}^{n} T_j^*=0; \tag{28}$$

with

$$T_j^*=\sum_{q=1}^{n_y/2}(a_{qi}^*A_q+\beta_{qi}^*B_q+\gamma_{qi}^*C_q+\delta_{qi}^*D_q); \tag{29}$$

for $i-n_p+n_y=1,2,\ldots,n_y$, where the coefficients α_{qi}^*, β_{qi}^*, γ_{qi}^* and δ_{qi}^* are extrapolations of α_{ijq}, β_{ijq}, γ_{ijq} and δ_{ijq} to $(x_w,y_i,0)$, and an extrapolation scheme on the two last panel layers is used, since the potentials are evaluated at the panel centroids. In this way, the algebraic problem is closed, since there are $N=n+2n_y$ equations and unknowns. There are *n active* panels, as rows and unknowns of the matrix equation and $2n_y$ nonlocal absorbing equations, where usually $n_y \ll n$.

7 Asymmetry of Dawson Methods

In order to understand how symmetry is broken in the Dawson-like methods, some properties of the related finite-difference operators should be taken in account. A very comprehensive analysis is shown by Letcher [25]. In these methods the free surface flow is considered to be a small perturbation of the double-body flow, which satisfies a zero normal velocity boundary condition on the hydrostatic equilibrium plane $z=0$. A linear free-surface boundary condition is derived and applied at $z=0$. The flow is then modeled with Rankine source panels placed over both the hydrostatic wetted body surface and a limited portion of the plane $z=0$. On each body panel, the usual Neumann boundary condition is applied and over each free surface panel, a Dawson-like boundary condition supplies one linear equation in the source densities. A key element is the use of upstream finite difference operators to approximate derivatives occurring in the free-surface boundary condition. By means of two-dimensional tests with a variety of difference operators, Dawson found that: (i) centered operators produce solutions exhibiting waves both upstream and downstream; (ii) operators using upstream points succeeded in suppressing upstream waves; (iii) the damping of the downstream wave depend strongly on the choice of the difference operator and on the Froude number; and (iv) a very particular upstream four-point operator (in a velocity formulation) gives near zero damping over a range of moderate speeds. The Dawson boundary condition for the perturbed flow discards all quadratic terms and can be written as

$$2UU_{,x}\tilde{u}+U^2\tilde{u}_{,x}+g\tilde{w}=-2U^2U_{,x} \quad \text{on } z=0 \tag{30}$$

where U is the x-component of the double-body velocity, $\tilde{u}=u-U$, $\tilde{w}=w-W$ are the perturbations on the velocity, with (u,w) as the components of the total (perturbed) velocity. As is noticed by Letcher, the Dawson scheme is an *irrational* approximation in the van Dyke *sense*, since it is not exact in any known limit and does not possess any small parameter allowing terms to be asymptotically ordered, so there is little rational basis to decide which terms to include and which to discard, aside from empirical demonstrations. In case that the double-body velocity U on $z=0$ is constant, e.g. if there is no body or the body is far away, then (30) reduces to the fully linearized free-surface boundary condition

$$\tilde{u}_{,x}+K\tilde{w}=0 \quad \text{on } z=0 \tag{31}$$

with $K=g/U_\infty^2$, and this is invariant under the longitudinal coordinate inversion symmetry $x\rightarrow -x$. In order to break it, the standard Rayleigh procedure is to introduce an *artificial* viscosity ν as

$$\tilde{u}_x+K\tilde{w}+\nu\tilde{u}=0 \quad \text{on } z=0. \tag{32}$$

This artificial viscosity is a small constant (with dimensions of the reciprocal of a length), which eventually approaches zero, and has the effect of moving a pole slightly off the integration path during evaluation of integrals that arise with an equivalent analysis by means of the Green functions and complex variable theory. This artifice is widely regarded as a reliable way to satisfy the radiation boundary conditions. The difference operator for numerical differentiation may be derived from the Taylor series. For data uniformly spaced, the Taylor series about x gives

$$f(x+nh)=\sum_{k=0}^{\infty}\frac{1}{k!}(nh)^k f^{(k)}(x); \tag{33}$$

a difference operator for the first derivative has the form of the weighed sum of several ordinates

$$\frac{df}{dx}\approx h^{-1}\sum_{n=-\infty}^{+\infty} p_n f(x+nh); \tag{34}$$

substituting (33) and reversing the order of the summations

$$\frac{df}{dx}\approx\sum_{k=0}^{+\infty} e_k h^{k-1} f^{(k)}(x); \tag{35}$$

where

$$e_k=\frac{1}{k!}\sum_n p_n n^k \tag{36}$$

is the coefficient of the kth derivative in (35). For a first-derivative operator it is suitable to make $e_0=0$ and $e_1=1$, by suitable choice of the w_n (e.g., see [25] for more details). Thus, the effect of using one of the difference formulas in place of the exact derivative in (32), is to introduce an infinite series of new terms involving various higher derivatives of u

$$\tilde{u}_{,x}+\sum_{k=2}^{+\infty} e_k h^{k-1}(\partial_x)^k\tilde{u}+K\tilde{w}+\nu\tilde{u}=0. \tag{37}$$

If the solution far downstream is assumed in the form

$$\begin{cases}\tilde{u}\sim e^{\tilde{K}z}\sin(\tilde{K}x);\\ \tilde{w}\sim e^{\tilde{K}z}\cos(\tilde{K}x);\end{cases} \tag{38}$$

then (37) conduces to

$$\begin{cases}K=\tilde{K}(1-e_3\beta^2+e_5\beta^4-e_7\beta^6+..); & (39a)\\ \nu=\tilde{K}(e_2\beta^1-e_4\beta^3+e_6\beta^5-..) & (39b)\end{cases}$$

where $\beta=\tilde{K}h$. The parameter Kh is 2π over the number of surface panels per wavelength, so (39a) shows that if the e_k are small and Kh is not too large, then, the perturbed wavenumber $\tilde{K}$ would be equal to K within $O(K^2h^2)$. The strong effect of the odd terms in the error is thus a small modification of the wavelength. On the other hand, (39b) shows that the even terms act exactly like a (speed-dependent) artificial viscosity ν needed to exactly offset the damping effects of the error terms. As Letcher remarks, the Dawson-like methods usually break down at higher Froude number (lower Kh) because the strong decline in the magnitude of νh allows upstream waves, but the breakdown has nothing to do with the question of whether these methods are low-speed theories owing to its basis in a double-body linearization. It is the upstream differencing that fails, not the double-body linearization.

8 Asymmetry of the Wave Expansion

The same procedure can be used for the asymptotic wave expansion. For simplicity, a velocity formulation is used and the linearized free surface boundary condition (32) is rewritten as

$$u_{q,x}+Kw_q+\nu u_q=0 \quad \text{on } z=0. \tag{40}$$

where $u_q=\tilde{\mu}_{,x}$ and $w_q=\tilde{\mu}_{,z}$ are the perturbed (modal) velocities. At far downstream, the wave expansion (38) is assumed and (39) is again obtained. The centered three-point difference operator using the points at $n=-1,0,+1$ has the weights $(p_0,p_1,p_2)=$

$(-1/2,0,1/2)$, its odd terms e_{2k+1} are all nulls, but not its even terms e_{2k}. Then, from (39), both perturbed and unperturbed wavenumber are equals, $\tilde{K}=K$, while the (speed-dependent) artificial viscosity ν remains. In other words, the proposed wave expansion (indirectly) satisfy the absorbing boundary conditions and, with a centered difference free-surface operator, no error is introduced in the wavenumber K.

9 Numerical Examples

9.1 Wigley Hull. The hull shape for the model 1805 A, e.g., see Dawson [7], is given by $\eta^{\pm}=\pm(1-\xi^2)(1-0.6\xi^2)(1-\zeta^2)$, with $\xi=2x/L$, $\eta=2y/B$ and $\zeta=z/H$, where H,B,L are the length, beam and draft of the model, respectively. The prismatic coefficient is defined as $C_p=\Omega/(LS)$ and the wave-resistance coefficient employed is the Circular Froude Coefficient $C_w=F_x/F_0$, with $F_0=(\pi/250)\rho U_\infty^2\Omega^{2/3}$, where Ω is the volume and S the area of the midship section. For this model $\Omega=(88/225)LBH$, $S=(2/3)BH$ and $C_p=44/75\approx 0.587$, respectively. The panel mesh employed, see Fig. 2, covers the free surface of the basic flow with 60×20 quadrilaterals, the wetted hull with about 1800 triangles and a vertical wall with 20×40 quadrilaterals, there are 20 panel strips, 40-Fourier modes and 3000 total unknowns. Fig. 3 shows the wave resistance coefficient plot obtained with the proposed method, compared with Shearer results (from Wehausen [26]), where: (i) the computed curve tends to be less in mean value than the experimental curves; (ii) the humps and the hollows in the computed curve are especially marked in comparison with the experimental one and (iii) the humps and the hollows occur

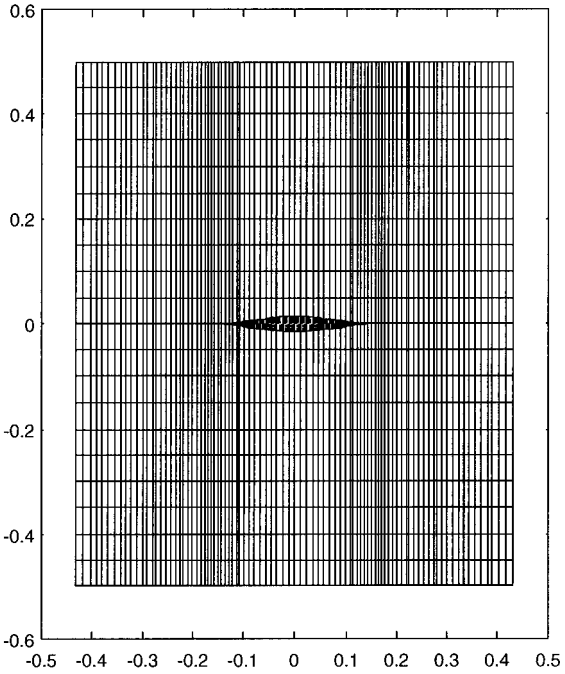

Fig. 2 A structured panel mesh over the free surface, around a Wigley model (*xy*-view)

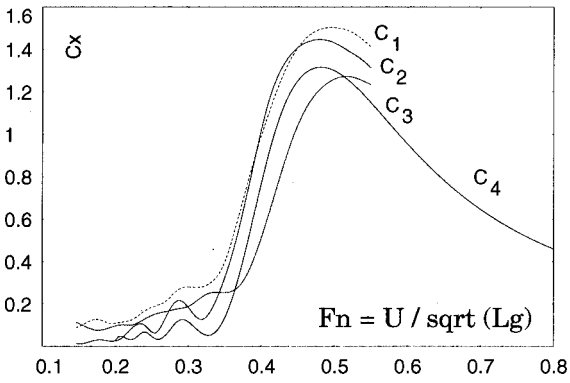

Fig. 3 Wave resistance coefficient for the Wigley model 2891: C_1: residuary for model free to trim, C_2: residuary for model fixed, C_3: calculated Michell resistance (from Wehausen [26], Fig. 20, p. 182); C_4: Panel-Fourier computation.

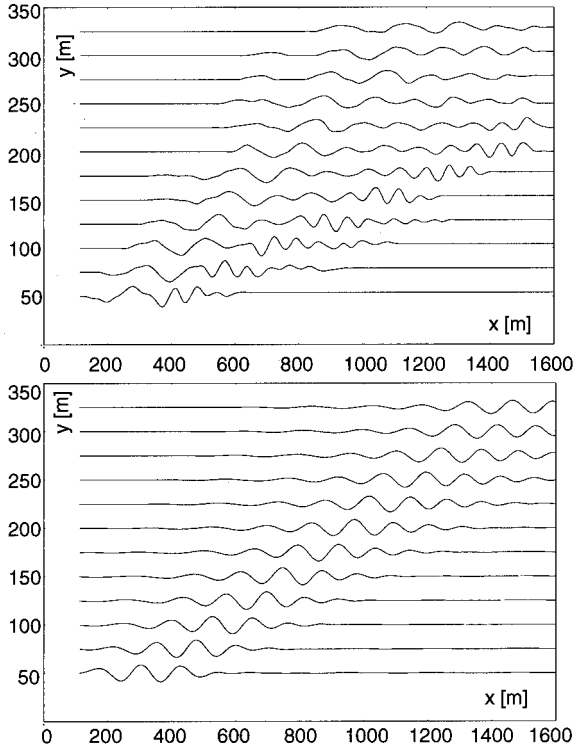

Fig. 4 Wave profiles at 40 knots ferry speed (magnification factor=10), top: from sensor measurements each 25 m on planes parallel to the gallery one, bottom: from a Panel-Fourier computation.

Table 1 Scatter table of the significant wave height H_z as a function of the zero crossing period T_z, at 10 knots, for 10 selected measured waves at each distance. Threshold level $t=0.05$.

Y_{50}	T_z	2.70	2.40	1.80	1.90	3.08	2.70	2.55	3.05	3.08	3.15
	H_z	0.08	0.11	0.06	0.06	0.06	0.14	0.14	0.06	0.06	0.05
Y_{75}	T_z	2.60	2.40	1.92	2.22	3.15	2.88	2.53	2.60	3.10	2.97
	H_z	0.10	0.11	0.05	0.07	0.06	0.07	0.11	0.17	0.12	0.10
Y_{100}	T_z	2.60	2.50	2.28	2.25	2.15	2.33	2.80	2.50	2.63	2.58
	H_z	0.09	0.10	0.06	0.06	0.05	0.07	0.08	0.14	0.11	0.08
Y_{125}	T_z	2.60	2.53	2.50	2.53	2.22	2.55	2.95	2.80	2.72	2.75
	H_z	0.05	0.08	0.10	0.07	0.06	0.07	0.07	0.14	0.14	0.13
Y_{150}	T_z	2.60	2.47	2.42	2.47	2.75	2.58	3.13			
	H_z	0.07	0.07	0.06	0.11	0.10	0.10	0.05			
Y_{175}	T_z	2.70	2.70	2.53	2.42	2.65	3.08	2.40	2.72	2.30	3.25
	H_z	0.05	0.08	0.08	0.07	0.06	0.08	0.13	0.07	0.07	0.06
Y_{200}	T_z	2.42	2.58	2.63	2.40	2.95	2.45	2.53	2.90	2.35	3.22
	H_z	0.05	0.08	0.09	0.06	0.05	0.11	0.15	0.08	0.07	0.07
Y_{225}	T_z	2.63	2.63	2.60	2.53	2.80	2.70	2.53	2.35	2.92	
	H_z	0.07	0.08	0.07	0.07	0.07	0.09	0.12	0.06	0.08	
Y_{250}	T_z	2.63	2.67	2.45	2.45	2.65	2.80	2.53	2.35	2.47	2.95
	H_z	0.07	0.09	0.07	0.08	0.10	0.09	0.11	0.08	0.07	0.07
Y_{275}	T_z	2.60	2.58	2.53	2.42	2.70	2.85	2.55	2.80	3.00	3.28
	H_z	0.07	0.07	0.06	0.07	0.09	0.09	0.09	0.07	0.06	0.05
Y_{300}	T_z	2.72	2.85	2.65	2.53	2.50	2.55	2.85	2.70	2.30	
	H_z	0.06	0.07	0.07	0.05	0.09	0.11	0.09	0.08	0.06	
Y_{325}	T_z	2.70	2.65	2.55	2.50	2.42	2.60	2.88	2.67	2.92	
	H_z	0.05	0.06	0.05	0.06	0.08	0.09	0.09	0.08	0.05	

Table 2 Scatter table of the significant wave height H_z as a function of the zero crossing period T_z, at 40 knots, for 10 selected measured waves at each distance. Threshold level $t = 0.20$.

Y_{50}	T_z	7.70	3.47	3.00	3.72	6.78	11.93	10.93			
	H_z	1.67	1.41	0.71	0.44	0.24	0.22	0.24			
Y_{75}	T_z	8.52	5.38	3.80	3.53	2.97	3.00	8.45	10.32		
	H_z	1.12	0.96	1.51	0.77	0.35	0.32	0.27	0.23		
Y_{100}	T_z	9.48	8.93	4.53	3.38	3.80	4.15	2.75	2.58	3.15	10.00
	H_z	1.02	0.76	0.99	1.32	0.84	0.45	0.27	0.21	0.21	0.20
Y_{125}	T_z	10.07	7.82	5.05	4.78	3.60	3.35	3.92	3.60	2.90	
	H_z	0.69	0.97	0.84	0.93	1.45	0.91	0.32	0.44	0.31	
Y_{150}	T_z	8.55	5.22	6.38	4.03	3.58	3.50	3.50	3.72	3.47	
	H_z	1.03	0.41	0.58	0.84	1.24	1.16	0.45	0.20	0.38	
Y_{175}	T_z	9.13	6.43	6.13	4.80	4.47	3.53	3.35	3.70		
	H_z	0.90	0.58	0.46	0.41	0.78	1.09	1.10	0.70		
Y_{200}	T_z	7.65	5.40	6.53	4.35	4.15	3.85	3.35			
	H_z	0.79	0.38	0.43	0.37	0.84	1.03	1.11			
Y_{225}	T_z	10.98	8.57	5.20	6.97	4.43	5.50	3.67			
	H_z	0.60	0.86	0.43	0.60	0.23	0.54	0.47			
Y_{250}	T_z	8.98	8.60	5.93	6.25	4.78					
	H_z	0.88	0.51	0.47	0.34	0.29					
Y_{275}	T_z	9.25	7.78	5.60	8.80						
	H_z	0.83	0.70	0.29	0.49						
Y_{300}	T_z	10.05	8.30	5.82	6.50						
	H_z	0.59	0.76	0.38	0.47						
Y_{325}	T_z	10.23	8.50	7.05	5.90						
	H_z	0.45	0.82	0.50	0.41						

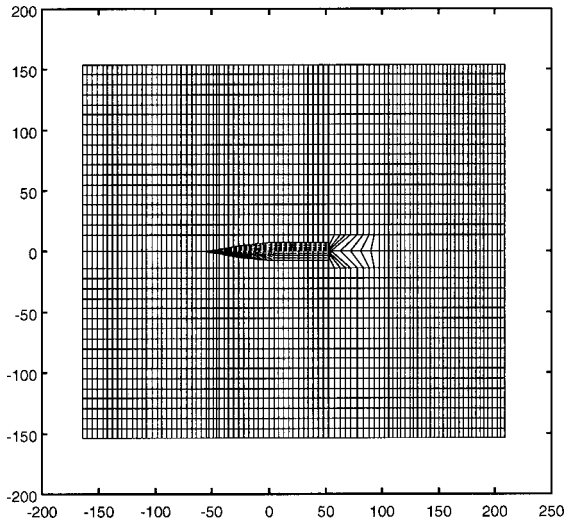

Fig. 5 Structured panel mesh on the free surface, around a ferry (*xy*-view)

rather earlier in the computed curve than in the experimental data. Note that the whole set of secondary maxima is clearly captured, extending to Froude numbers as low as 0.2. On the other extreme, Froude numbers as high as 0.8 are computed without problems, while standard methods like those derived from Dawson suffer from some reflections specially at high Froude numbers.

9.2 Transport Ferry. Tests of the wave-height profile, at 40 equivalent knots, have been performed for a model of transport ferry, in scale (1:25) made of glass fiber and ballasted in order to reproduce the displacement, mean draft and trim corresponding to the real ship. The main model dimensions are: displacement with appendices=1.11 kN, length between perpendiculars=4.4 m, beam of trace=0.588 m, and draft mean=0.095 m. The vessel channel is 150×30×5 m and possesses a planar motion carriage for the dragging and controlling of the model. The water depth in the tests was 5 m equivalent to 125 m at real scale, therefore it can be considered to correspond to deep water. The model was dragged from its center of mass following rectilinear trajectories in such a way that it allows vertical and dynamic trim motions. The measurements were done by means of three resistive sensors to elevation of the free surface, located at fixed points of the central zone of the channel, as to avoid reflections on the walls, and over a same transversal line to the channel, separated at a distance of 2 m between them, equivalent to 50 m at full scale. Four passages at 2, 3, 8, and 9 m between the gallery plane and the nearest sensor were done. In this form the wake was measured between 50 and 325 m with intervals of 25 m at real scale, in planes parallel to the gallery plane of the ship. The wake-profiles

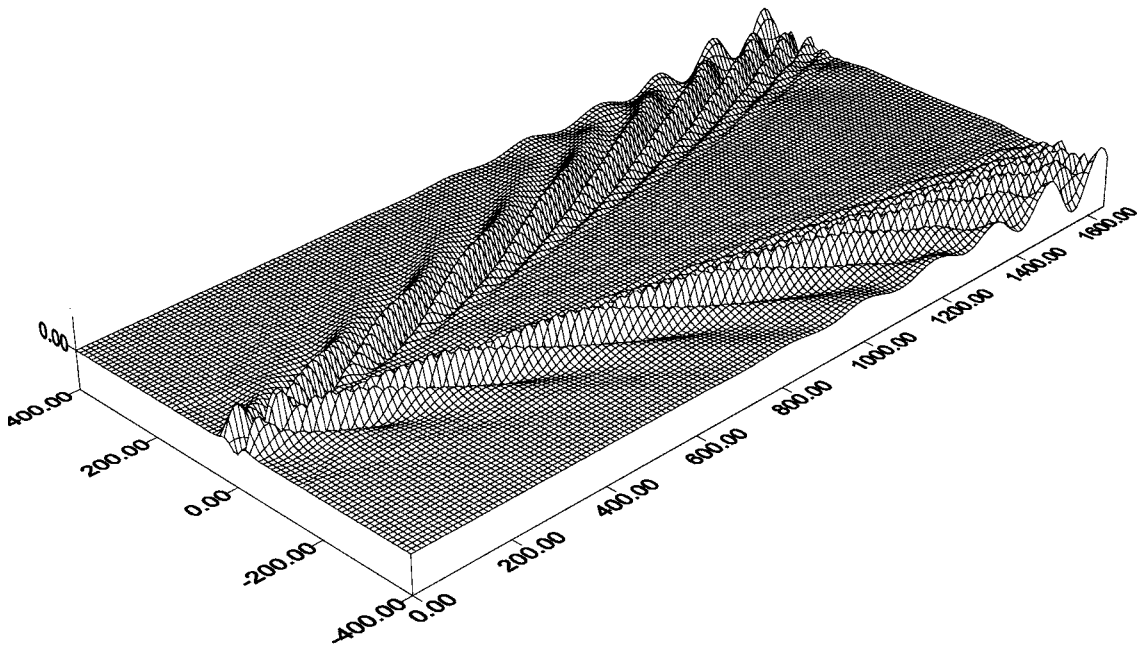

Fig. 6 Perspective view of the wave-pattern for a ferry at 40 knots along 15 ship-lengths, computed with the Fourier series

measured are shown at the top of Fig. 4. Ten measures were selected from the greater zero-crossing waves at each distance, where the measured waves that were smaller than a threshold were discarded in order to reduce interference effects, surface irregularities and noise. The threshold level was varied for each velocity due to the different magnitude of the wake height. The plots of the significant wave height as a function of the zero crossing period (scatter diagrams) are shown in Tables 1 and 2. In the calibration of the wave-resistive sensors, the display constant was of 0.731 mm/point and the sensor constant resulting was -15 V/m. Each sensor generates a proper wave which is a function of the velocity and kind of the measured wave, but in any case was greater than 2 mm. In these tests, the proper wave was measured in vacuum ($<$0.5 mm) and, then, was subtracted to the measured senial. The panel mesh, see Fig. 5, covers: the free surface of the basic flow with 90×36 quadrilaterals, the wetted hull with 438 triangles and a vertical wall with 36×18 quadrilaterals, resulting 3678 active panels, $n_y=36$ panel strips, 72 Fourier modes and 3750 total unknowns. Once a numerical solution over the computational free surface is obtained, the wave-pattern behind the vertical wall may be computed by means of a post-processing computation with the finite Fourier representation of the asymptotic wave-potential coupled to the dispersive relation. The initial data is the wave-potential and its x derivative at the panel strip behind the ship. At the bottom of Fig. 4 the numerical wave-height profiles of the wake are shown, which are found with the post-processing procedure at the same planes as the measured ones, with a reasonable comparison between measured and computed wave-heights profiles, except, of course, near to the transom-stern due to vorticity effects. It is also noted that it can go back as far as 15 lengths in the downstream direction and 3 lengths in the beam one, with a negligible computational effort as compared with a direct strategy of trying to cover this surface with panels. Finally, in Fig. 6 a perspective view of the computed wake is shown.

10 Conclusions

The ship-like flow problem has been considered by means of a three-dimensional potential model and a linearized free-surface boundary condition. This problem has been numerically solved by a panel method coupled with a finite Fourier series. In contrast with the Dawson-like methods, a second centered difference scheme has been used for the free-surface discrete operator. Centered schemes reduce the numerical viscosity in the discretization in such a way that, no error is introduced in the wavenumber while the (speed-dependent) artificial viscosity remains. The wave-resistance has been computed by a pressure integration over the static wetted hull, and the wave-heights in the downstream free surface behind the artificial boundary, have been obtained as a post-processing procedure, therefore, it can go fairly far behind the ship with a lower computational cost than a direct strategy of covering the free surface with panels. This procedure enables to consider significantly smaller meshes for the free surface, and the computation can be done over a broad interval of the Froude number. The overall approach is limited by the restrictions of the potential flow model and the use of a structured free surface mesh. Future modeling efforts would be focused on this area as well as on coupling the hydrodynamic model with a boundary layer solver for a viscous/inviscid interaction.

Acknowledgment

This work was supported by *Consejo Nacional de Investigaciones Científicas y Técnicas* (CONICET, Argentina) and *Banco Interamericano de Desarrollo* through grant BID 802/OC-AR PID 26. The work was partially performed with *Free Software Foundation/GNU-Project* resources. The experimental data was provided by *Centro Internacional de Métodos Numéricos en Ingeniería* (CIMNE, Barcelona) and *Canal de Experiencias Hidrodinámicas de El Pardo* (CEHIPAR, Madrid). The authors thank the referees for their constructive suggestions and careful reading.

Appendix: Linearized Boundary Conditions

A linearized dynamic boundary condition is developed first. At the 0,1-stages (basic and perturbed flows), the potentials are $\mathbf{\Phi}_{0,1}=\mathbf{u}_\infty^T\mathbf{x}+\phi_{0,1}$. Their gradient modules are

$$U_{0,1}^2=u_\infty^2+2\mathbf{u}_\infty^T\mathbf{u}_{0,1}+u_{0,1}^2; \tag{41}$$

where $\mathbf{U}_{0,1}=\nabla\mathbf{\Phi}^{0,1}$ and $\mathbf{u}_{0,1}=\nabla\phi^{0,1}$. Then

$$\Delta U^2=2\mathbf{u}_\infty^T\Delta\mathbf{u}+\Delta u^2; \tag{42}$$

where $\Delta U^2=U_1^2-U_0^2$, $\Delta\mathbf{u}=\mathbf{u}_1-\mathbf{u}_2$ and $\Delta u^2=u_1^2-u_0^2$. Expanding ϕ_1 and η_1 at first order in ε

$$\begin{cases}\varepsilon\psi=\phi_1-\phi_0; & (43a)\\ \varepsilon\eta=\zeta^1-\zeta^0. & (43b)\end{cases}$$

Then $\mathbf{u}_1=\mathbf{u}_0+\varepsilon\nabla\psi$ and

$$\Delta u^2=2\varepsilon\mathbf{u}_0^T\nabla\psi+\varepsilon^2|\nabla\psi|^2. \tag{44}$$

Introducing (44) in (42)

$$\Delta U^2=2\varepsilon\mathbf{U}_0^T\nabla\psi+O(\varepsilon^2). \tag{45}$$

The Bernoulli equations at the 0,1-stages are

$$\frac{1}{2}U^{0,1}+g\zeta^{0,1}=\frac{1}{2}u_\infty^2+r^{0,1}\quad\text{at}\quad\Gamma^{0,1}; \tag{46}$$

where $r^{0,1}$ are the 0,1-residuals since in an asymptotic iterative process it is assumed that the dynamic condition is not fully verified. The difference is

$$\frac{1}{2}\Delta U^2+g\Delta\zeta=\Delta r\quad\text{at}\quad\Gamma^{0,1} \tag{47}$$

where $\Delta\zeta=\zeta_1-\zeta_0$ and $\Delta r=r_1-r_0$. Introducing (43*b*) and (45)

$$\varepsilon(\mathbf{U}_0^T\nabla\psi+g\eta)+O(\varepsilon^2)=\Delta r \tag{48}$$

since $\mathbf{U}_0$ is evaluated at Γ^0 and $\nabla\phi^{0,1}$ are evaluated at $\Gamma^{0,1}$, it should be known the location of the two boundaries $\Gamma^{0,1}$, but a simplified procedure can be introduced by means of a transfer calculus (e.g., Reference [10]). For if we only consider known boundaries, all flow variables are transferred to Γ_0, then $\phi_1(\mathbf{x}')\approx\phi_1(\mathbf{x})$ and $\psi^1(x')\approx\psi^1(\mathbf{x})$ plus terms $O(\varepsilon)$, i.e., a simple boundary displacement. All terms in Eq. (48) are evaluated at Γ^0 and Eq. (3.3) is obtained.

Next, a linearized kinematic boundary condition is obtained. The basic free surface Γ^0 is the plane $z=0$, whereas the perturbed one Γ^1 can be written as $z=\varepsilon\eta(x,y)$, and will be near it for ε small enough. Over the plane $z=0$ the unit normal $\mathbf{n}(\mathbf{x})=(0,0,1)$ is constant, and over the perturbed one $\mathbf{n}(\mathbf{x}')=(-\varepsilon\eta_{,x},-\varepsilon\eta_{,y},1)$, at first order on ε. Its change can be written as

$$\delta\mathbf{n}(x)=\mathbf{n}(\mathbf{x}')-\mathbf{n}(\mathbf{x})=(-\varepsilon\eta_{,x},-\varepsilon\eta_{,y},0) \tag{49}$$

where $\mathbf{x}'\in\Gamma^1$ and $\mathbf{x}\in\Gamma^0$. The transfer of the gradient is considered by

$$\nabla\phi_1(\mathbf{x}')=\nabla\phi_1(x)+\nabla\nabla^T\phi_1(\mathbf{x})\mathbf{n}(\mathbf{x})\eta\varepsilon. \tag{50}$$

Introducing (43) and since $\nabla\nabla^T\phi^{0,1}$ are assumed symmetric, resulting

$$\nabla^T\phi_1(\mathbf{x}')=\nabla^T\phi_0(\mathbf{x})+\nabla^T\psi(\mathbf{x})\varepsilon+\mathbf{n}^T(\mathbf{x})\nabla\nabla^T\phi_0(\mathbf{x})\eta\varepsilon+O(\varepsilon^2). \tag{51}$$

The perturbed kinematic boundary condition and unit normal are

$$\begin{cases}\nabla^T\phi_1(\mathbf{x}')\mathbf{n}(\mathbf{x}')=0 & (52a)\\ \mathbf{n}(\mathbf{x}')=\mathbf{n}(\mathbf{x})+\delta\mathbf{n}(\mathbf{x}). & (52b)\end{cases}$$

Introducing (51) and (52b) into (52a)

$$\nabla^T\phi_1\mathbf{n}=\nabla^T\phi_0\mathbf{n}+\nabla^T\psi\mathbf{n}\varepsilon+\nabla^T\phi_0\delta\mathbf{n}+\mathbf{n}^T(\nabla\nabla^T\phi_0)\mathbf{n}\eta\varepsilon+O(\varepsilon^2). \tag{53}$$

where the left and right side are evaluated at $\mathbf{x}'$ and $\mathbf{x}$, respectively. The boundary velocity in the basic flow is contained by the plane $z=0$ and then $\nabla^T\phi_0\mathbf{n}=0$. Now

$$\nabla^T\phi_0\delta\mathbf{n}=-\varepsilon\eta_{,x}\phi_{0,x}-\varepsilon\eta_{,y}\phi_{0,y}+O(\varepsilon^2). \tag{54}$$

For the last term, it can be written $\mathbf{n}^T(\nabla\nabla^T\phi_0\mathbf{n})=\mathbf{n}^T\mathbf{t}$, where

$$t_i=\frac{\partial^2\phi_0}{\partial x_i\partial x_j}n_j=\frac{\partial}{\partial x_i}\left(\frac{\partial\phi_0}{\partial x_j}n_j\right) \tag{55}$$

for $i,j=1,2,3$, employing Einstein summation convention over repeated indices and it has been taken into account that $\mathbf{n}(\mathbf{x})=(0,0,1)$ is a constant vector. This is reduced to

$$\frac{\partial}{\partial x_i}\left(\frac{\partial\phi_0}{\partial x_j}n_j\right)=\left[\frac{\partial}{\partial x}\frac{\partial\phi_0}{\partial z},\frac{\partial}{\partial y}\frac{\partial\phi_0}{\partial z},\frac{\partial}{\partial z}\frac{\partial\phi_0}{\partial z}\right]. \tag{56}$$

The z-component of the velocity field $u_{0z}=\partial_z\phi_0$ over all the plane $z=0$ is null, then $\partial_x(u_{0z})=\partial_y(u_{0z})=0$ at $z=0$ and

$$\frac{\partial}{\partial x_i}\left(\frac{\partial\phi_0}{\partial x_j}n_j\right)=\left[0,0,\frac{\partial^2\phi_0}{\partial z^2}\right]\quad\text{at}\quad z=0 \tag{57}$$

collecting these partial results

$$\epsilon\left(\frac{\partial\psi}{\partial n}+\eta\frac{\partial^2\phi_0}{\partial z^2}-\frac{\partial\eta}{\partial x}\frac{\partial\phi_0}{\partial x}-\frac{\partial\eta}{\partial y}\frac{\partial\phi_0}{\partial y}\right)+O(\epsilon^2)=0 \tag{58}$$

since ϕ_0 is harmonical in Ω^0, then $\phi_{0,zz}=-\phi_{0,xx}-\phi_{0,yy}$ and, at first order,

$$-\frac{\partial\psi}{\partial n}+\frac{\partial}{\partial x}\left(\eta\frac{\partial\phi_0}{\partial x}\right)+\frac{\partial}{\partial y}\left(\eta\frac{\partial\phi_0}{\partial y}\right)=0\quad\text{at}\quad z=0. \tag{59}$$

References

[1] Morino, L., and Kuo, C. C., 1974 ''Subsonic Potential Aerodynamics for Complex Configurations: A General Theory,'' AIAA J. **12**, pp. 191–197.

[2] Katz, J., and Plotkin A., 1991, *Low-Speed Aerodynamics, From Wing Theory to Panel Methods*, Mcgraw-Hill.

[3] Mokry, M., 1990, ''Complex Variable Boundary Element Method for External Potential Flows,'' *28th Aerospace Sciences Meeting*, January 8–11, Reno, Nevada.

[4] Storti, M., D'Elía, J., and Idelsohn, S., 1995, ''CVBEM formulation for multiple profiles and cascades,'' Appl. Mech. Rev., **48**, No. 11, Part 2. pp. 203–210.

[5] Morino, L., ed., 1985, *Computational Methods in Potential Aerodynamics*, Springer-Verlag.

[6] Kinnas, S. A., and Hsin, C. Y., 1992, ''Boundary Element Method for the Analysis of the Unsteady Flow Around Extreme Propeller Geometries,'' AIAA J., **30**, pp. 688–696.

[7] Dawson, C. W., 1977, ''A Practical Computer Method for Solving Ship-Wave Problems'' *2nd Int. Conf. on Numerical Ships Hydrodynamics*, Berkeley, CA, pp 30–38.

[8] Farmer, J., Martinelli, L., and Jameson, A., 1994, ''Fast Multigrid Method for Solving Incompressible Hydrodynamic Problems with Free Surfaces,'' AIAA J., **32**, No. 6, June, pp. 1175–1182.

[9] Stoker, J. J., 1957, *Water Waves*, Interscience, New York.

[10] van Dyke, M., 1975, *Perturbation Methods on Fluid Mechanics*, Parabolic Press, Stanford.

[11] Newman, J. N., 1978, ''The Theory of Ship Motions,'' Appl. Mech. **18**, pp. 221–283.

[12] Baumann, C., Storti, M., and Idelsohn, S., 1992, ''A Petrov-Galerkin technique for the solution of transonic and supersonic flows,'' Comput. Methods Appl. Mech. Eng., **95**, pp. 49–70.

[13] Nigro, N., Storti, M., and Idelsohn, S., 1995, ''Fluid flows around turbomachinery using an explicit pseudotemporal Euler FEM code,'' J. Commun. Numer. Methods Eng., **11**, pp. 199–211.

[14] Givoli, D., 1991, ''Non-reflecting Boundary Conditions,'' J. Comput. Phys., **94**, pp. 1–29.

[15] Bonet, R., Nigro, N., Storti, M., and Idelsohn, S., 1998, ''A Discrete Non-Local (DNL) Outgoing Boundary Condition for Diffraction of Surface Waves,'' Commun. Numer. Methods Eng., **14**, pp. 849–861.

[16] Storti, M., D'Elía, X., and Idelsohn, S., 1998, ''Algebraic Discrete Non-Local (DNL) Absorbing Boundary Condition for the Ship Wave Resistance Problem,'' J. Comput. Phys., **146**, No. 2, pp. 570–602.

[17] Storti, M., D'Elía, J., and Idelsohn, S., 1998, ''Computing Ship Wave Resistance from Wave Amplitude with the DNL Absorbing Boundary Condition,'' Commun. Numer. Methods Eng., **14**, pp. 997–1012.

[18] Storti, M. , D'Elía, J., Bonet, R., Nigro, N., and Idelsohn, S., 2000 ''The DNL Absorbing Boundary Condition. Applications to Wave Problems,'' Comput. Meth. Appl. Mech. Eng. **182**, (3-4), pp. 483–498.

[19] Broeze, J., and Romate, J. E., 1992, ''Absorbing Boundary Conditions for Free Surface Wave Simulations with a Panel Method,'' J. Comput. Phys., **99**, pp. 146–158.

[20] Medina, D. E., and Liggett, J. A., 1988, ''Three-Dimensional Boundary Element Computation of Potential Flow in Fractured Rock,'' Int. J. Numer. Methods Eng., **26**, pp. 2319–2330.

[21] D'Elía J., 1997, ''Numerical Methods for the Ship Wave-Resistance Problem,'' Ph.D. thesis, Univ. Nacional del Litoral, Santa Fe, Argentina.

[22] D'Elía, J., Storti, M., and Idelsohn, S., 2000 ''Iterative solution of panel discretizations for potential flows. The modal/multipolar preconditioning,'' Int. J. Numer. Methods Fluids, **32**, No. 1, pp. 1–27.

[23] D'Elía, J., Storti, M., and Idelsohn, S., 2000 ''Smoothed Surface Gradients for Panel Methods,'' Adv. Eng. Soft. **31**, No. 5, pp. 327–334.

[24] D'Elía, J., Storti, M., and Idelsohn, S., 2000, ''A Closed Form for Low Order Panel Methods,'' Adv. Eng. Software **31**, No. 5, 335–341.

[25] Letcher, J. S., 1993, ''Properties of finite-difference operators for the steady-wave problem,'' J. Ship Res., **37**, No. 1, Mar., pp. 1–7.

[26] Wehausen, J. V., 1973, ''The Wave Resistance of Ships,'' Adv. Appl. Mech., **13**, pp. 93–245.